Biochimica et Biophysica Acta 1818 (2012) 2707–2717

Contents lists available at SciVerse ScienceDirect

Biochimica et Biophysica Acta

journal homepage: www.elsevier.com/locate/bbamem

Molecular characterization of the interaction of crotamine-derived nucleolar targeting peptides with lipid membranes

Margarida Rodrigues [a,1], Andrea Santos [a,1], Beatriz G. de la Torre [b], Gandhi Rádis-Baptista [b,c], David Andreu [b], Nuno C. Santos [a,*]

[a] Instituto de Medicina Molecular, Faculdade de Medicina da Universidade de Lisboa, Lisbon, Portugal
[b] Department of Experimental and Health Sciences, Pompeu Fabra University, Barcelona Biomedical Research Park, Barcelona, Spain
[c] Laboratório de Bioquímica e Biotecnologia, Instituto de Ciências do Mar, Universidade Federal do Ceará, Fortaleza, Brazil

ARTICLE INFO

Article history:
Received 6 December 2011
Received in revised form 8 June 2012
Accepted 20 June 2012
Available online 28 June 2012

Keywords:
Nucleolar-targeting peptide
Crotamine
Cell-penetrating peptide
Membrane partition
Membrane translocation
Fluorescence spectroscopy

ABSTRACT

A novel class of cell-penetrating, nucleolar-targeting peptides (NrTPs), was recently developed from the rattlesnake venom toxin crotamine. Based on the intrinsic fluorescence of tyrosine or tryptophan residues, the partition of NrTPs and crotamine to membranes with variable lipid compositions was studied. Partition coefficient values (in the 10^2–10^5 range) followed essentially the compositional trend POPC:POPG ≤ POPG < POPC ≤ POPC:cholesterol. Leakage assays showed that NrTPs induce minimal lipid vesicle disruption. Fluorescence quenching of NrTPs, either by acrylamide or lipophilic probes, revealed that NrTPs are buried in the lipid bilayer only for negatively-charged membranes. Adoption of partial secondary structure by the NrTPs upon interaction with POPC and POPG vesicles was demonstrated by circular dichroism. Translocation studies were conducted using a novel methodology, based on the confocal microscopy imaging of giant multilamellar vesicles or giant multivesicular liposomes. With this new procedure, which can now be used to evaluate the membrane translocation ability of other molecules, it was demonstrated that NrTPs are able to cross lipid membranes even in the absence of a receptor or transmembrane gradient. Altogether, these results indicate that NrTPs interact with lipid bilayers and can penetrate cells *via* different entry mechanisms, reinforcing the applicability of this class of peptide as therapeutic tools for the delivery of molecular cargoes.

1. Introduction

Some specific cationic peptides and proteins, usually rich in lysine and arginine residues and with the ability to translocate cell membranes, have found use as intracellular delivery agents. Due to their translocating properties, they were named cell-penetrating peptides (CPPs) more than two decades ago [1–4]. CPPs can be covalently conjugated or complexed with a variety of payloads, such as nucleic acids, proteins, nanoparticles or quantum dots [5–7], enabling their use in a broad range of applications, including transfection, siRNA technology, organelle imaging or delivery of low-permeability drugs [8–10]. The most studied CPPs in terms of cell translocation and effectiveness as biomedical agents are the HIV-1 transcriptional activator (Tat) [1], the antennapedia homeodomain from *Drosophila* (Antp) [11], and the VP22 protein from the Herpes simplex virus [12]. More recently, Kerkis et al. [13] reported the cell-penetrating ability of crotamine, a 42-amino acid cationic defensin-like polypeptide from the venom of South American rattlesnake (*Crotalus durissus terrificus*), and described, among other properties, its uptake by proliferating active human and murine embryonic stem cells *in vitro* and mouse cells *in vivo*. The NMR solution structure of crotamine [14] revealed as main features a short N-terminal α-helix (residues 1–7) and two anti-parallel β-sheets (residues 9–13 and 34–38), giving rise to an αββ fold stabilized by three intramolecular disulfide bonds. This type of fold was previously identified on other membrane-active peptides, such as the human antimicrobial peptide β-defensin 2 [15], platypus defensin-like peptide [16], scorpion α-toxins [17] and anemone anthopleurin-B [18]. Based on such structural data, a molecular dissection of crotamine allowed to define a minimal CPP pharmacophore [19] involving the splicing of the 1–9 and 38–42 segments (Fig. 1) and giving rise to a novel class of CPPs whose unexpected localization led to their naming of nucleolar targeting peptides (NrTPs). NrTPs retain the cell-penetrating peptide property of crotamine

Abbreviations: Ahx, 6-aminohexanoic acid; AMP, antimicrobial peptide; CD, circular dichroism; CF, 5,(6)-carboxyfluorescein; CPPs, cell penetrating peptides; DLS, dynamic light scattering; DPPE, 1,2-dipalmitoyl-*sn*-glycero-3-phosphoethanolamine; Fmoc, 9-fluorenylmethoxycarbonyl; GUV, giant unilamellar vesicles; HEPES, 4-(2-hydroxyethyl)-1-piperazineethanesulfonic acid; HPLC, High-performance liquid chromatography; LUV, large unilamellar vesicles; NBD, nitro-2-1,3-benzoxadiazol-4-yl; NMR, nuclear magnetic resonance; NrTPs, nucleolar-targeting peptides; 5-NS, 5-doxyl-stearic acid; 16-NS, 16-doxyl-stearic acid; POPC, 1-palmitoyl-2-oleoyl-*sn*-glycero-3-phosphocholine; POPG, 1-palmitoyl-2-oleoyl-*sn*-glycero-3-phospho-(19-*sn*-glycerol); RhB, rhodamine B

* Corresponding author at: Unidade de Biomembranas, Instituto de Medicina Molecular, Faculdade de Medicina da Universidade de Lisboa, Av. Prof. Egas Moniz, 1649-028 Lisbon, Portugal. Tel.: +351 217999480; fax: +351 217999477.
E-mail address: nsantos@fm.ul.pt (N.C. Santos).

[1] Contributed equally to this work.

0005-2736/$ – see front matter © 2012 Elsevier B.V. All rights reserved.
doi:10.1016/j.bbamem.2012.06.014

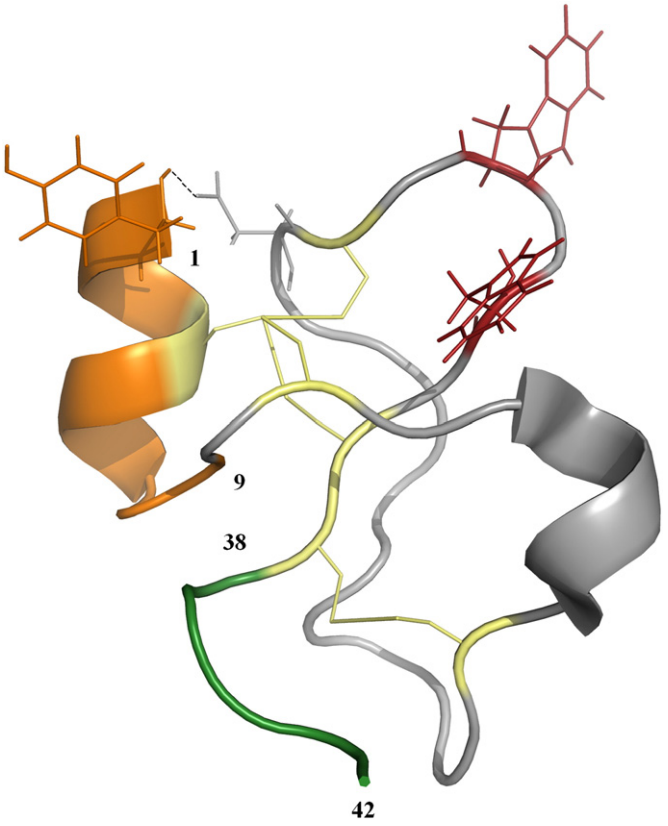

Fig. 1. Crotamine structure (PDB ID: 1Z99), showing the spliced regions, N-terminal residues 1–9 (orange) and C-terminal residues 38–42 (green), disulfide bonds (yellow), Trp_{32} and Trp_{34} (red), and H-bond between Tyr_1 and Asp_{29} (- - - -).

and present several improvements, such as reduced toxicity, preferential nucleolar localization and reduced synthesis cost [18,19]. We have recently reported their ability to deliver large cargoes (e.g., the 465 kDa β-galactosidase tetramer) into mammalian cells [20].

To gain insight into the biophysical aspects of the interaction of NrTPs with lipid bilayers, we carried out a systematic study of the molecular determinants underlying the CPP behavior of NrTPs, particularly concerning the involvement of specific types of lipids. The extent of NrTPs and crotamine partition into model membranes (including zwitterionic and anionic lipids), as well as their ability to translocate lipid bilayers, have been evaluated. The presence of aromatic amino acid residues on NrTPs and crotamine allowed the use of fluorescence spectroscopy to assess peptide:membrane interaction. Fluorescence quenching by acrylamide and lipophilic quenchers informed about peptide location on the membrane. Vesicle leakage was studied by monitoring the release of the fluorescent probe 5,(6)-carboxyfluorescein (CF) induced by NrTPs or crotamine. On the translocation studies, the uptake of rhodamine B-labeled NrTPs by giant lipid vesicles was examined by confocal microscopy.

2. Materials and methods

2.1. Materials

1,2-dipalmitoyl-*sn*-glycero-3-phosphoethanolamine-nitro-2-1, 3-benzoxadiazol-4-yl (DPPE-NBD), 1-palmitoyl-2-oleoyl-*sn*-glycero-3-phosphocholine (POPC) and 1-palmitoyl-2-oleoyl-*sn*-glycero-3-phospho-(19-*sn*-glycerol) (POPG) were obtained from Avanti Polar Lipids (Alabaster, AL). 5,(6)-Carboxyfluorescein, cholesterol, 4-(2-hydroxyethyl)-1-piperazineethanesulfonic acid (HEPES), NaCl and Triton X-100 were from Sigma (St. Louis, MO). Acrylamide, tris(hydroxymethyl)aminomethane hydrochloride (Tris–HCl), L-tryptophan, L-tyrosine, sucrose and glucose were from Merck (Darmstadt, Germany). 5-Doxyl-stearic acid (5-NS) and 16-doxyl-stearic acid (16-NS) were obtained from Aldrich (Milwaukee, WI). All reagents were used without further purification.

2.2. Peptides

The synthesis of NrTP1 (YKQCHKKGGKKGSG), NrTP2 (with a 6-aminohexanoic acid spacer between GG and KK) and NrTP5 (as NrTP1, but with D-amino acid residues) was described earlier [19]. Similar protocols were used for the synthesis of NrTP6 (Cys residue replaced by Ser, see Table 1), NrTP7 (all 5 Lys residues changed to Arg) and NrTP8 (Tyr replaced by Trp). Amino acid sequences, molar extinction coefficients, quantum yields and molecular masses are also given in Table 1. All peptides were prepared both with free and rhodamine B (RhB)-labeled N-termini, the latter versions to be used in translocation experiments.

Synthetic crotamine in the native folding pattern was prepared from a linear precursor made by Fmoc solid phase synthesis methods as described before for similar multiple disulfide peptides [21]. Oxidative folding of the HPLC-purified hexathiol precursor, dissolved at 5 μM concentration in 0.1 M ammonium acetate, pH 7.8, was done in the presence of 1 M guanidinium chloride and reduced (GSH) and oxidized (GSSG) glutathione (1:100:10 peptide:GSH:GSSG molar ratio), under Ar atmosphere, for 48 h. A single oxidation product was obtained with the expected molecular mass and HPLC retention time of a natural crotamine sample. Further details are given as Supplementary Information.

2.3. Characterization of crotamine and NrTPs in solution

UV–vis absorption and fluorescence (both excitation and emission) spectral characterization of NrTPs (25–97 μM) and crotamine (7.7 μM) were carried out in 10 mM HEPES with 150 mM NaCl, pH 7.4. This buffer was used in all experiments, except when mentioned otherwise. Quantum yields were calculated as described by Fery-Forgues et al. [22].

2.4. Lipid vesicle preparation

Large unilamellar vesicles (LUV) with ~100 nm diameter were obtained by extrusion of multilamellar vesicles, as described elsewhere [23]. LUV of pure POPC and POPG, POPC:POPG 70:30 (mol%) and POPC: cholesterol 67:33 (mol%) were used on the peptide–membrane interaction and translocation studies. Giant unilamellar vesicles (GUV) were prepared by the electroformation method, as described elsewhere [24,25]. POPC and DPPE-NBD stock solutions were mixed to a final lipid concentration of 1 mM (1% NBD-DPPE) and hydrated with ~1 mL of 200 mM sucrose. After GUV preparation, the vesicles suspension was kept at room temperature in the dark until use. Independent of the method used to prepare GUV (gentle hydration or electroformation), a small percentage of non-unilamellar vesicles is formed [26]. These vesicles can be either multilamellar (when the entrapped vesicles are concentric; hereafter named giant multilamellar vesicles, GMLV) or multivesicular (when the entrapped vesicles are non-concentric and significantly smaller; hereafter named giant multivesicular liposomes, GMVL). Translocation experiments were conducted using these two types of non-unilamellar giant vesicles.

2.5. Extent of partition to membranes

Membrane partition studies were carried out using an Edinburgh Instruments steady-state fluorescence spectrophotometer Xe 900 (Livingston, UK). NrTPs and crotamine solutions concentrations were checked by UV/Vis absorption using the extinction coefficients on Table 1, and

Table 1
Sequence, molecular mass, molar absorptivity (ε) and fluorescence quantum yield (ϕ) of crotamine and crotamine-derived NrTPs.

Peptide	Sequence[a]	Molecular mass[b]	ε ($M^{-1}cm^{-1}$)[c]	ϕ	Description
Crotamine	YKQCHKKGGHCFPKE KICLPPSSDFGKMDCR WRWKCCKKGSG	4883.86 (4883.80)	10,400		
NrTP1	YKQCHKKGGKKGSG	1505.53 (1505.76)	1506	0.019	(1–9)–(38–42) residues of crotamine
NrTP2	YKQCHKKGGXKKGSG	1619.01 (1618.92)	1086	0.028	Insertion of 6-aminohexanoic acid (X)
NrTP5	ykqchkkGGkkGsG	1505.49 (1505.76)	1882	0.059	NrTP1 with D-amino acid residues
NrTP6	YKQSHKKGGKKGSG	1489.26 (1489.70)	827	0.052	NrTP1 with Cys→Ser replacement
NrTP7	YRQSHRRGGRRGSG	1629.16 (1628.84)	963	0.033	NrTP6 with Lys→Arg replacement
NrTP8	WKQSHKKGGKKGSG	1511.83 (1511.75)	3143	0.123	NrTP6 with Tyr→Trp replacement

[a] All peptides are C-terminal carboxyls, with a net charge of +5 at physiological pH (assuming ca. 50% protonation of His). The N-terminal rhodamine B-labeled versions of the six NrTPs were also available.
[b] Determined by MALDI-TOF mass spectrometry; theoretical mass in parenthesis.
[c] Determined at 275 and 280 nm for Tyr- and Trp-containing peptides, respectively.

varied between 7.7 μM and 97 μM ($Abs_{280\ nm}$ ~0.08–0.1). Small volumes of LUV suspensions (15 mM) were successively added to the peptide or protein samples. After 10 min incubation, the fluorescence spectra were recorded using an excitation wavelength (λ_{exc}) of 280 nm (5 nm bandwidth) and emission wavelengths (λ_{em}) in the interval from 295 nm to 500 nm (5 nm or 10 nm bandwidth). All spectra were corrected for the response of the fluorescence detecting system, Raman scattering and dilution effect. Tryptophan and tyrosine fluorescence quenching at high lipid concentrations was corrected as described elsewhere [27]. All measurements were repeated at least twice.

Partition coefficients, K_p, were calculated assuming two models (for reviews on these and other formalisms see [28–30]): (i) simple partition; and, (ii) peptide self-quenching [7]. In the simple partition model experimental fluorescence intensity data (I) were fitted with [28]:

$$\frac{I}{I_W} = \frac{1 + K_p \gamma_L \frac{I_L}{I_W}[L]}{1 + K_p \gamma_L [L]} \quad (1)$$

where I_W and I_L are the fluorescence intensities with all the fluorophores in aqueous solution or inserted in the lipid membrane, respectively, γ_L is the molar volume of the phospholipid and [L] the lipid concentration. For the peptide self-quenching model, experimental data were fitted with [7]:

$$\frac{I}{I_W} = \frac{K_p \gamma_L \frac{I_L}{I_W}[L]}{1 + K_p \gamma_L [L] + k_2 K_p I_L} + \frac{1}{1 + K_p \gamma_L [L]} \quad (2)$$

where k_2 is proportional to the ratio between the bimolecular self-quenching rate and the radiative decay rate.

2.6. Fluorescence quenching experiments

Acrylamide was used as a peptide fluorescence quencher in steady-state experiments. 5-NS and 16-NS were used both in steady-state and time-resolved measurements. The quenching experiments mediated by acrylamide were performed using a Varian Cary Eclipse fluorescence spectrophotometer (Mulgrave, Australia). Experimental settings were λ_{exc} = 284 nm or 295 nm (5 nm bandwidth), to minimize the quencher light absorption and inner-filter effect, and λ_{em} = 303 nm or 355 nm (5 nm or 10 nm bandwidth), for Tyr and Trp containing peptides, respectively. Acrylamide was added to the peptide solution up to 226 mM. Peptide solutions were prepared using Abs_{275nm} = 0.1 for Tyr containing peptides and Abs_{280nm} = 0.06 for the Trp containing ones. Experiments were conducted in the presence and absence of lipid vesicles (up to 1 mM). Control experiments were preformed with free Tyr and Trp, with or without lipid vesicles. Fluorescence intensity data were corrected using the formalism presented by Coutinho et al. [31], in order to account for the inner-filter effect.

Acrylamide is a collisional quencher; therefore, the quenching process can be described by the Stern–Volmer relationship [32]:

$$\frac{I_0}{I} = 1 + K_{SV}[Q] \quad (3)$$

where I_0 and I are the fluorescence intensities in the absence and presence of a concentration of quencher [Q], respectively. K_{sv} is the Stern–Volmer constant, which is related to k_q, the bimolecular quenching rate constant, and τ_0, the fluorophore fluorescence lifetime in the absence of quencher, by:

$$K_{SV} = k_q \tau_0 \quad (4)$$

Stern–Volmer plots with negative deviations from linearity were analyzed using the Lehrer model (for reviews see, [31,33]):

$$\frac{I_0}{I} = \frac{1 + K_{SV}[Q]}{(1 + K_{SV}[Q])(1 - f_B) + f_B} \quad (5)$$

where:

$$f_B = \frac{I_0^B}{I_0} \quad (6)$$

is the fraction of initial fluorescence intensity emitted by the fluorophores accessible to the quencher.

5-NS or 16-NS quenching experiments were conducted by adding small aliquots of the quencher stock solutions (70 mM in ethanol) to solutions with 35 μM NrTP8 and 3 mM POPC or POPG vesicles, after a 10 min incubation. The final ethanol concentration was kept below 2% (v/v) to avoid lipid bilayer perturbations [34]. On steady-state measurements, emission spectra were recorded from 305 nm to 500 nm (10 nm bandwidth), with excitation at 290 nm (5 nm bandwidth) in order to minimize the quencher to tryptophan absorption ratios. Raman scattering, dilution and inner-filter effects were taken into account on the spectral correction. Positive deviations from linearity in Stern–Volmer plots were analyzed using the quenching sphere-of-action model [35]:

$$\frac{I_0}{I} = 1 + K_{SV}[Q]e^{V[Q]} \quad (7)$$

where V is the static quenching constant.

Time-resolved intensity decays were obtained by pulse excitation at 280 nm (vertically polarized) and fluorescence acquired at 350 nm (20 nm bandwidth, at magic angle, 54.7°), using a 20 ns time span and 1024 channels in a multichannel analyzer. These measurements were performed in a time-resolved fluorescence equipment LifeSpec

II from Edinburgh Instruments, using a picosecond pulsed LED for excitation.

The fluorescence lifetimes were obtained from intensity decay fits with a sum of exponentials and using a nonlinear least-squares method based on the Marquardt algorithm [36]. The quality of the fits was evaluated from χ^2 values, distributions of the residuals and autocorrelation plots. Time-resolved quenching data was analyzed using the same equations and assuming:

$$\frac{I_0}{I e^{V[Q]}} = \frac{\bar{\tau}_0}{\bar{\tau}} \tag{8}$$

where $\bar{\tau}$ is the average fluorescence lifetime, and $e^{V[Q]} = 1$ in the absence of static quenching. On the studies of quenching by the lipophilic molecules 5-NS or 16-NS, the effective quencher concentration in the membrane was calculated as previously described [37], using the partition coefficients of the quenchers $K_{p,5\text{-NS}} = 12570$ and $K_{p,16\text{-NS}} = 3340$ [38].

2.7. Dynamic light scattering studies

Dynamic light scattering (DLS) measurements were conducted on a Malvern Zetasizer Nano ZS (Malvern, UK) with a backscattering detection at 173°, equipped with a He-Ne laser ($\lambda = 632.8$ nm), at 25 °C, using disposable polystyrene cells. Pure POPG was diluted to a final concentration of 50 μM and then filtered through a sterile 0.45 μm pore size filter (Whatman, Florham Park, NJ). NrTP1 was added to the lipid vesicles at the final concentrations of 3.3 μM and 5.0 μM (lipid:peptide ratios 1:15 and 1:10, respectively). Normalized intensity autocorrelation functions were analyzed using the CONTIN method [39–41], yielding a distribution of hydrodynamic diameters (D_H). A set of 15 measurements (~13 runs each) was carried out for the lipid vesicles in the absence and presence of each NrTP1 concentration.

2.8. Lipid vesicle leakage assays

NrTP-induced lipid vesicle leakage experiments were done as described elsewhere [23,41,42], using a Varian Cary Eclipse fluorescence spectrophotometer. Briefly, the release of 5,(6)-carboxyfluorescein (CF) entrapped in LUV was monitored by fluorescence dequenching. Different concentrations of NrTPs (0–20 μM) or crotamine (0–4 μM) were incubated with CF-entrapping LUV (10 μM, in 20 mM Tris–HCl with 150 mM NaCl, pH 7.4.), at 25 °C. Fluorescence was recorded continuously during 30 min, with constant stirring, using $\lambda_{exc} = 492$ nm and $\lambda_{em} = 517$ nm. After 27 min, 1% (v/v) Triton X-100 was added to the vesicles for complete disruption. The percentage of leakage was determined by [42]:

$$\%leakage = \frac{I_F - I_{F,0}}{I_{F,100\%} - I_{F,0}} \tag{9}$$

where I_F and $I_{F,0}$ are the fluorescence intensities in the presence and absence of peptides, respectively, before the addition of Triton X-100, and $I_{F,100\%}$ is the fluorescence intensity after Triton X-100 addition. All fluorescence intensities were corrected for dilution.

2.9. Circular dichroism

Circular dichroism (CD) spectra were obtained using a JASCO spectropolarimeter model J-815 (Tokyo, Japan), at 25 °C, in the 195–260 nm wavelength range, with a bandwidth of 2 nm and 0.1 cm quartz cells. Solutions of 70 μM NrTP8 were used in the absence or presence of 6 mM POPC or POPG LUV. Peptide samples were scanned at different concentrations in order to detect eventual aggregation effects. Results were expressed in terms of mean residue ellipticity, [θ], according to [43]:

$$[\theta] = \frac{\theta}{Nlc} \tag{10}$$

where θ is the observed ellipticity, N is the number of amino acids in the peptide, l is the path length and c is the peptide concentration. The final spectra were the average of ten measurements after subtraction of buffer or vesicles baselines. Spectra analysis, to predict the peptide secondary structure, was done using the K2d software (http://www.embl.de/~andrade/k2d/) [44].

2.10. Translocation assays

Translocation experiments were carried out using a Zeiss confocal point-scanning microscope model LSM 510 META (Jena, Germany). Argon (488 nm; 45 mW) and diode-pumped solid-state (DPSS; 561 nm; 15 mW) lasers were used with a 63× oil-objective of 1.4 numerical aperture. For these assays, 15 μM rhodamine B-labeled peptides (NrTPs-RhB) were used and tested with GUV, GMLV and GMVL of POPC with 1% NBD-DPPE. Giant vesicles were diluted 1:2.6 (v/v) in 200 mM glucose and placed in 8-well plates for 30 to 60 min (μ-slide 8 well, uncoated, from Ibidi, Munich, Germany), where they were allowed to sediment by gravity. Plates were placed under the microscope, where they stabilized for 10–15 min before measurements start upon peptide addition. The method to detect and quantify translocation was based on the detection of rhodamine B inside the vesicles and on the co-localization of labeled peptides with inner giant vesicle membranes (Fig. 2). RhB labeling of these membranes occurs only when the peptide is able to translocate across the external vesicle bilayer, accessing the inner bilayers. Images were processed using Zeiss software and Image J (rsbweb.nih.gov/ij/).

3. Results and discussion

3.1. Crotamine and NrTPs spectral characterization

At room temperature and pH 7.4, crotamine and NrTP8 peptide absorption maxima are at 280 nm due to the Trp residues. Their fluorescence emission spectra have maxima at 345 nm (Fig. 3), typical of Trp exposed to the aqueous environment. In fact, both crotamine tryptophan residues have their indole rings fully exposed to the solvent (Fig. 1). For NrTPs 1–7, the absorption maxima are at 275 nm. When excited at 280 nm, the fluorescence emission spectra of these peptides have maxima at 302 nm, except for NrTP5, where an emission maximum at 306 nm was observed (Fig. 3). These values are typical for Tyr fluorescence on proteins and polypeptides without Trp residues [45].

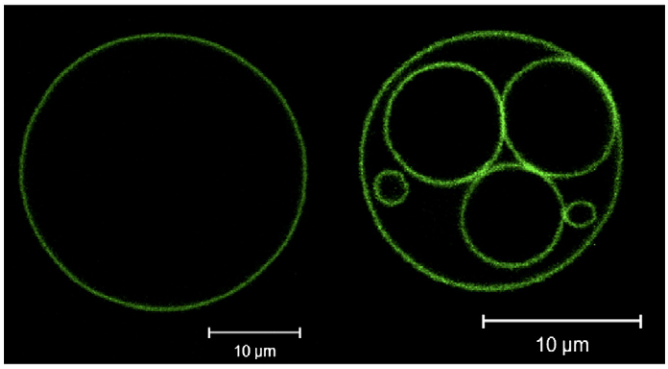

Fig. 2. Giant unilamellar vesicle (left) and giant multilvesicular liposome (right) used for NrTPs translocation studies. Membranes of POPC labeled with NBD (1%). Green fluorescence is detected by confocal microscopy upon excitation with 488 nm laser.

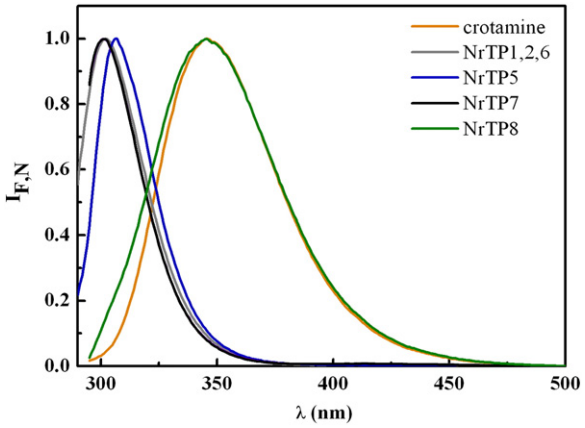

Fig. 3. Normalized fluorescence emission spectra of crotamine 7.7 μM and NrTPs (25–97 μM) obtained at λ_{exc} = 280 nm, pH 7.4, 25 °C.

3.2. Molecular partition assays

Table 2 summarizes the values obtained for the partition coefficients (K_p), ratios between the fluorescence intensities in aqueous solution and in lipid (I_L/I_w) and models used to fit the partition data. Fig. 4 presents the partition curves obtained for crotamine and NrTP1. The partition curve patterns of the other NrTPs are similar and can be found as Supplementary Information.

Two types of zwitterionic lipid bilayers were used in these studies: pure POPC and POPC:cholesterol 67:33 (mol%). Pure POPC bilayers are in the liquid disordered state. The addition of cholesterol increases the lipid acyl chain ordering, leading to the formation of a liquid ordered phase [46–49]. These zwitterionic lipid systems were used to mimic the outer leaflets of mammalian cell membranes. POPC is a 1-saturated, 2-unsaturated phosphatidylcholine (PC), a common motif in the naturally occurring phospholipids, being the major component in PC isolated from several natural sources [50]. Negatively charged lipid bilayers, such as those of pure POPG or POPC:POPG 70:30 (mol%), were used to simulate bacterial membranes [51] and to analyze the contribution of charge effects for the peptide–membrane interaction. The content of anionic phospholipids on bacterial membranes is within the 30–40% range [52]. Pure POPG was used for the sake of comparison and to assess the effect of an increase on the percentage of negatively-charged phospholipids.

Crotamine partition curves are well described by the simple partition model and were fitted with Eq. (1) (Table 2 and Fig. 4A). The protein–lipid interactions are characterized by high partition coefficients and I_L/I_w ratios below 1 for all the lipid systems tested. Crotamine global net charge at pH 7.4 is +10. However, this charge, seems not to be the major determinant for the crotamine–lipid interaction, as the K_p values obtained for the interaction with POPG-containing bilayers are only slightly higher than those obtained for zwitterionic membranes. Furthermore, crotamine extent of partition is higher for the POPC:POPG mixture than for pure POPG, probably as a result of both hydrophobic and electrostatic forces acting together. The high K_p values obtained for POPC and POPC:cholesterol vesicles agree well with crotamine high capacity to interact with mammalian cells [13]. The 7 nm blue shift on the emission maxima at [L] > 0.2 mM and the decrease on I_L/I_w observed for the crotamine partition to POPG vesicles are due to a change on crotamine tryptophan residues micro-environment, which becomes more hydrophobic upon interaction with the bilayer. No spectral shifts were observed on other crotamine–lipid partitions, indicating that on these cases Trp residues are partially exposed to the aqueous environment upon membrane binding. The addition of cholesterol to the POPC bilayers had no significant effect on the partition coefficient, showing that crotamine has no particular preference to (or exclusion from) cholesterol-rich membrane domains. The decrease in Trp quantum yield upon peptide interaction with lipid vesicles (opposing to the most common increase of the quantum yield), gives rise to the observed downward partition curves. The same behavior has been previously observed for human and plant defensins, which fold similarly to crotamine [53,54]. The three disulfide bonds on the Trp vicinity may account for most of its quenching, since cystines are strong Trp emission quenchers [55]. Upon protein–membrane interaction, crotamine structure rearranges and cystines should come closer to the Trp residue quenching its fluorescence more efficiently.

As crotamine, NrTP1 shows high affinity for zwitterionic membranes, with and without cholesterol (Table 2 and Fig. 4B). These results agree with the observations of Rádis-Baptista et al. [19], describing the interaction and translocation of this and other NrTPs into HeLa cells. The partition is reduced in approximately one order of magnitude for negative LUV ($K_{p,POPG} = 1.5 \times 10^3$ and $K_{p,POPC:POPG} = 2.3 \times 10^3$), despite the peptide positive net charge (+5). However, it is important to bear in mind that, even with such a decrease, the peptide still presents a considerably high partition for these membranes. The NrTP1-POPG interaction is also characterized by an upward curvature ($I_L > I_w$), at variance with the observed for all crotamine partitions and NrTP1 partition to zwitterionic membranes. Tyr residues quantum yield can be affected by several quenching mechanisms regarding their local environment in the peptide [45]. During the partition process, the residues on vesicles interface undergo distance and space orientation changes, affecting tyrosine emission. In the present case, the most probable quenching agents are: (*i*) the hydrated peptide carbonyl group; and, (*ii*) the sulfhydryl group of cysteine. The protonated charged forms of nearby Lys residues have no significant effect on Tyr fluorescence.

All NrTP1 partition curves were well fitted with Eq. (1), except for POPC:POPG, in which the more complex self quenching model (Eq. (2)) was necessary (Fig. 4B). In this case, a decrease on the peptide fluorescence quantum yield at low lipid concentrations was first observed, followed by an increase. High fluorophore concentrations in the membrane at low lipid concentrations usually account for this self-quenching phenomenon [7].

Adding a flexible 6-aminohexanoic acid (Ahx) spacer onto NrTP1 structure (NrTP2), to connect the peptide N- and C-terminal amino

Table 2
Crotamine and NrTPs partition coefficients (K_p) and ratio between the fluorescence intensities in aqueous solution and in lipid (I_L/I_w), for partitions to POPC, POPG, POPC:POPG 70:30 and POPC:cholesterol 67:33 LUV. Models used to fit the experimental results: SP—Simple Partition; SQ—Self Quenching (marked with *). Data are presented as the best fit value ± standard error.

	$K_p/10^3$				I_L/I_W				Model
	POPC	POPG	POPC:POPG	POPC:chol	POPC	POPG	POPC:POPG	POPC:chol	
Crotamine	22 ± 4	31 ± 4	44 ± 7	25 ± 4	0.69 ± 0.01	0.57 ± 0.01	0.80 ± 0.01	0.69 ± 0.01	SP
NrTP1	55 ± 17	1.5 ± 0.2	2.3 ± 0.7*	30 ± 9	0.90 ± 0.01	1.53 ± 0.03	1.25 ± 0.03	0.93 ± 0.00	SP; SQ (*)
NrTP2	12 ± 3	1.6 ± 0.4	3.9 ± 0.8*	23 ± 4	0.91 ± 0.00	1.56 ± 0.05	1.29 ± 0.03	0.89 ± 0.00	SP; SQ (*)
NrTP5	72 ± 18*	3.0 ± 0.7	9.2 ± 1.0	109 ± 19*	0.81 ± 0.01	1.57 ± 0.07	1.59 ± 0.01	0.78 ± 0.00	SP; SQ (*)
NrTP6	14 ± 5	1.8 ± 0.2	0.16 ± 0.04	170 ± 55	0.96 ± 0.00	1.98 ± 0.04	1.41 ± 0.07	0.94 ± 0.00	SP
NrTP7	31 ± 12	1.9 ± 0.4	0.15 ± 0.02	56 ± 21	0.95 ± 0.00	2.06 ± 0.06	2.30 ± 0.15	0.95 ± 0.00	SP
NrTP8	18 ± 6	2.4 ± 0.4	3.1 ± 1.1*	18 ± 5	0.84 ± 0.01	1.59 ± 0.02	1.17 ± 0.05	0.83 ± 0.01	SP; SQ(*)

acid residues, does not increase the membrane partition of this peptide. In fact, the partition coefficient of NrTP2 to POPC membranes decreases, while the I_L/I_w ratio is maintained. For POPG and POPC:POPG bilayers, the observed K_p and I_L/I_w values are similar to those obtained for NrTP1. In the case of NrTP5, the amino acid chirality factor is significantly relevant only for the interactions with POPC:cholesterol and POPC:POPG membranes, where K_p values are 4-fold higher than for NrTP1. Partition curves for POPC and POPC:cholesterol vesicles are better characterized by the self quenching model. In these cases, the higher K_p values lead to higher peptide local concentrations in the bilayer, and consequently to Tyr fluorescence quenching. For NrTP6, the Cys residue replacement by Ser reduces the partition extent to POPC and POPC:POPG bilayers, relative to NrTP1. The peptide partition into POPC:cholesterol, on the contrary, is highly favored. A similar trend was observed for the arginine-rich NrTP7 peptide partition curves. For NrTP8 (replacement of Tyr by a Trp residue), the extent of partition into POPG or POPC:POPG is lower than for POPC or POPC:cholesterol vesicles, as observed for NrTP1. Blue shifts of 9 nm and 16 nm, for NrTP8-POPC:POPG and NrTP8-POPG interactions, respectively, were observed, as noticed for crotamine. This clearly indicates that the Trp region interacts with the membrane, reducing its exposure to the aqueous environment and, thus, increasing its quantum yield.

For all the studied NrTPs, the partition curve patterns vary between negative and zwitterionic bilayers, suggesting that the nature of the peptide–lipid interaction is different. Results for zwitterionic membranes show very high K_p values, associated with $I_L<I_W$ (indicative of quenching upon membrane binding), while partition into negative membranes seem to be associated with lower (but still high) K_p values, with the most common relation $I_L>I_W$. The peptide residues involved on the interaction with the bilayers vary with the ionic character of the membranes, zwitterionic or anionic. In fact, the peptides undergo conformational changes that dictate their affinity and location in the vesicles, at surface or buried on it. This observation is particularly highlighted by the experiments with NrTP8, where the Trp residue emission maximum is shifted, in a clear indication of medium polarity change. Also, the different I_L/I_w ratio values obtained for the POPC and POPG containing bilayers, points out for peptide conformational changes occurring upon interaction with the lipid surface. The significant differences among I_L/I_w ratios for the lipids tested, together with the decrease in K_p observed for zwitterionic lipid vesicles, reflect the preference of NrTPs to stay adsorbed in this lipid membrane. On the other hand, in POPG containing vesicles the extent of interaction was greater, indicating membrane penetration, driven mainly by electrostatic forces.

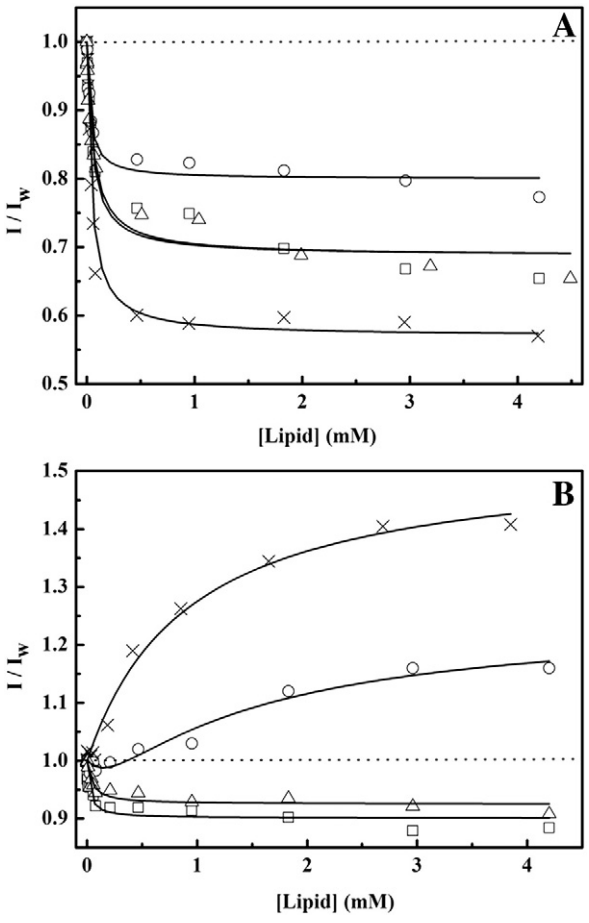

Fig. 4. (A) Crotamine 7.7 μM partition curves, fitted with Eq. (1), for POPC (□), POPG (×), POPC:POPG 70:30 (○) and POPC:cholesterol 67:33 (Δ) LUV. (B) NrTP1 53 μM partition curves, fitted with Eqs. (1) or (2), for LUV with the same lipid composition.

3.3. Fluorescence quenching experiments

Fluorescence quenching by acrylamide experiments were conducted for all peptides, in aqueous solution and in the presence of LUV (Table 3; Fig. 5). Acrylamide is often used to study the accessibility of peptide fluorophores to the aqueous environment. If the fluorophore of the peptide is fully shielded in the membrane, it becomes inaccessible to this aqueous quencher, which possesses a low capacity of penetration into lipid bilayers [56]. In solution, the Stern–Volmer plots of all studied peptides are linear (Fig. S8), indicating that there are no major aggregates in solution [57]. Acrylamide quenching in the presence of POPC vesicles revealed almost no variation in the K_{SV} value for all NrTPs, suggesting that the peptide fluorophore remains accessible to the quencher. The fraction of light emitted from the peptides that interact with the membrane (f_L) can be calculated from the K_p [37]:

$$f_L = \frac{\frac{I_L}{I_W} K_p \gamma_L [L]}{1 + \frac{I_L}{I_W} K_p \gamma_L [L]} \quad (11)$$

In the case of NrTP5 with 1 mM POPC vesicles, f_L is 99.8%. This result indicates that all the peptides are interacting with the membrane. On the other hand, f_B (fraction of light from flurophores accessible to the quencher; Eq. (6)) is 91% for the same system. This means that almost all peptide is accessible to the quencher (Table 3). Also for NrTP5, but with 1 mM POPG vesicles, f_L is reduced to 78%, with a f_B of 41%, indicating that approximately half of the peptide is shielded from acrylamide, *i.e.*, stays buried in the membrane. Thus, there is more peptide interacting with POPC than with POPG vesicles, but while for POPC the peptide is at the membrane surface, in POPG-containing systems it stays buried in the bilayer, protected from the quenching by acrylamide (Fig. 9). The same conclusions apply to NrTP8 and remaining peptides. The distinct behavior between NrTP5 and NrTP8 regarding POPC:POPG vesicles was also detected in the partition studies. NrTP8 interacts to a less extent with POPC:POPG compared to NrTP5, in agreement with the high values of f_B (~1) and K_{SV}. In general, only the presence of negatively charged vesicles induced a decrease in K_{SV}, which can be considered as an indication of membrane penetration.

To obtain more information on the in-depth location of NrTPs upon binding to a lipid membrane, 5-NS and 16-NS lipophilic probes were used to quench NrTP8 fluorescence in the presence of POPC or POPG vesicles (Fig. 6 and Table 4). The quencher doxyl moiety of 5-NS is located in a shallower position (closer to the lipid–water interface) than in 16-NS; therefore, 5-NS is a better quencher of molecules located near the membrane interface [58]. The quenching by both in-depth probes is more pronounced in the NrTP8-POPG system, where higher K_{SV} values were obtained. This agrees well with the results obtained using

Table 3
Quenching of NrTPs fluorescence by acrylamide in the presence and absence of lipid vesicles. LUV of POPC, POPG, POPC:POPG 70:30 and POPC:cholesterol 67:33 were used. K_{SV} and f_B were calculated using Eq. (3) (linear Stern–Volmer plots) or Eq. (5) (Stern–Volmer plots with negative deviation). Data are presented as the best fit value from two independent experiments ± standard error.

Quenching in solution								
Peptide	NrTP1	NrTP2	NrTP5	NrTP6	NrTP7	Tyr	NrTP8	Trp
K_{SV} (M^{-1})	7.48 ± 0.12	7.00 ± 0.05	13.84 ± 0.05	8.39 ± 0.15	8.34 ± 0.06	24.82 ± 0.66	20.81 ± 0.18	23.94 ± 0.27
Quenching in the presence of lipid vesicles								
Peptide	NrTP5				NrTP8			
Lipid	POPC	POPC:Chol	POPG	POPC:POPG	POPC	POPC:Chol	POPG	POPC:POPG
K_{SV} (M^{-1})	14.30 ± 0.86	12.75 ± 1.40	6.15 ± 0.75	6.41 ± 1.39	19.43 ± 0.68	24.9 ± 0.47	6.75 ± 0.66	15.95 ± 0.46
f_B	0.91 ± 0.02	0.92 ± 0.03	0.41 ± 0.03	0.44 ± 0.05	1	1	0.52 ± 0.02	1

acrylamide, where it was found that ~50% of the peptide population was buried in the POPG bilayer. In the case of POPC vesicles, the K_{SV} value for 16-NS is higher than for 5-NS, which seems to be at odds with the previous results (partition and acrylamide quenching) that show the peptides' preference to be adsorbed to the lipid–water interface upon interacting with zwitterionic membranes. However, it should be noted that the 16-NS quencher group has a broader transversal distribution in the membrane than the same moiety in 5-NS, with some of the 16-NS quencher groups transiently locating close to the lipid–water interface [59,60]. As a result, 16-NS (despite a low quenching efficiency) may quench more efficiently than 5-NS a fluorophore located at this interface.

The differences between the K_{SV} values obtained by steady-state and time-resolved fluorescence spectroscopy measurements account for static quenching effects. The close proximity between the fluorophore and the quencher molecule is the main cause for this phenomenon. In the steady-state experiments using 5-NS, data were fitted with the sphere-of-action model (Eq. (7)), from where a value for the static quenching constant, V, can be recovered (Table 4). The V values obtained, 4.44 M^{-1} for POPC and 1.08 M^{-1} for POPG, are consistent

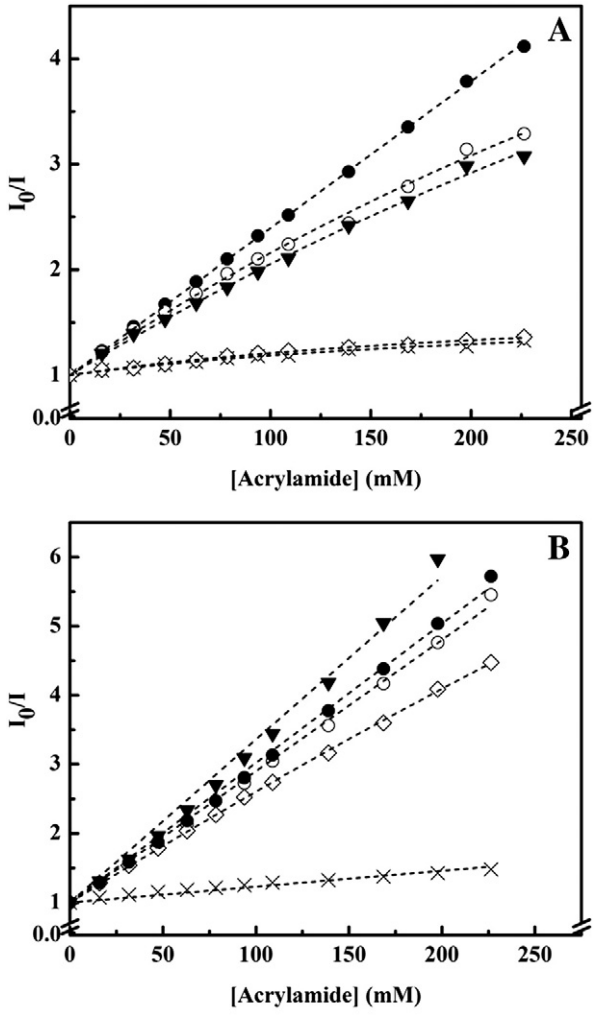

Fig. 5. Stern–Volmer plots of NrTP5 53 μM (A) and NrTP8 19 μM (B) quenching by acrylamide, in the absence (●), or presence of POPC (○), POPC:cholesterol (▼), POPC:POPG (◊) or POPG (×) LUV.

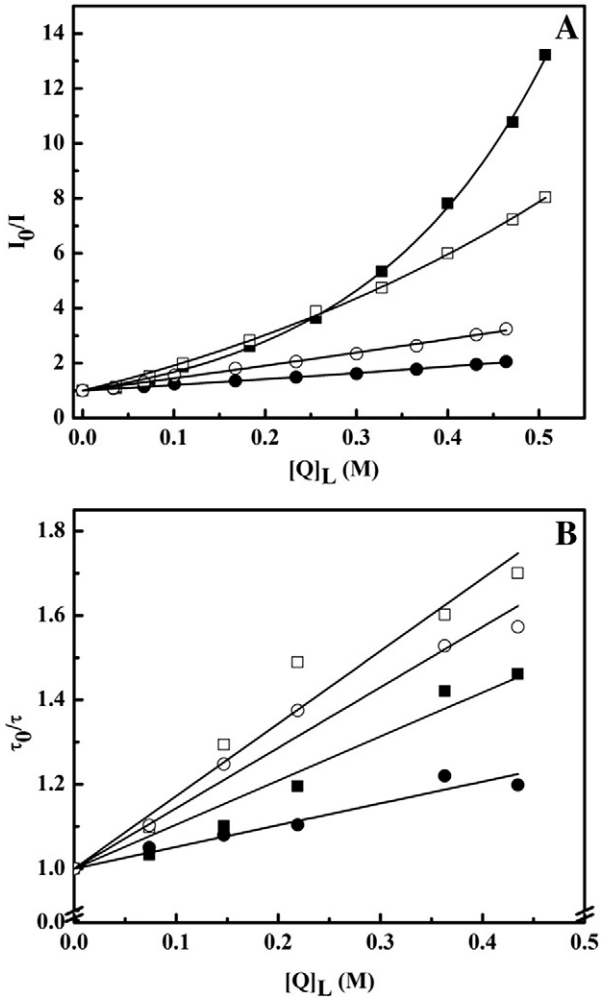

Fig. 6. Stern–Volmer plots of NrTP8 35 μM quenching by 5-NS (■,□) or 16-NS (●,○), in LUV of POPC (solid symbols) or POPG (open symbols), by using steady-state (A) and time-resolved (B) fluorescence spectroscopy data. Quencher concentrations are expressed as effective concentrations in the membrane [37].

Table 4
Stern–Volmer constant (K_{SV}), fraction of fluorophore emission accessible to the quencher (f_B), radius of the sphere of action (r_{SA}) and static quenching constant (V) for NrTP8 in POPC or POPG LUV, quenched by 5-NS or 16-NS. These values were obtained using Eq. (3) (linear Stern–Volmer plots) or Eq. (7) (Stern–Volmer plots with positive deviation; marked with *) to fit the experimental data.

	POPC		POPG	
	Steady-state	Time-resolved	Steady-state	Time-resolved
$K_{SV,\ 5\text{-}NS}$ (M^{-1})	0.75 ± 0.53*	1.04 ± 0.06	7.18 ± 0.44*	1.72 ± 0.10
$r_{SA,\ 5\text{-}NS}$ (Å)	12.24 ± 5.44	–	7.64 ± 3.57	–
$V_{5\text{-}Ns}$ (M^{-1})	4.44 ± 0.39	–	1.08 ± 0.11	–
$K_{SV,\ 16\text{-}NS}$ (M^{-1})	2.18 ± 0.03	0.57 ± 0.03	4.66 ± 0.07	1.43 ± 0.06

with a random distribution of quencher around the fluorophore, as it is in the aqueous phase [61]. For the NrTP8-POPC systems, most of the peptide rest in the vesicles surface. As a result, fluorophore quenching by both in-depth probes is much less efficient than by acrylamide, where higher K_{SV} values were observed (Table 3).

3.4. POPG aggregation in the presence of NrTPs

Light scattering studies were performed in order to test the possible aggregation of negatively charged lipid vesicles, promoted by the positively charged peptides. Results showed that the addition of NrTP1 to POPG vesicles promotes aggregation in a concentration dependent manner, as the peak of the size distribution histogram is shifted to the right (Supplementary Information; Fig. S10). Although the peptide:lipid ratio of 1:10 is the one yielding more and larger aggregates, for the ratio of 1:15 an increased polydispersion is already visible, which *per se* is a sign of the beginning of the aggregation process [62]. The aggregation of negatively charged vesicles triggered by NrTPs suggests that these peptides may also have antimicrobial activity. POPG vesicles can be seen in this context as an approximate model to bacterial membranes, once bacterial membranes are typically more anionic than mammalian cells membranes. Such an antimicrobial behavior would not be unexpected, since several CPPs possess also antimicrobial peptide (AMP) activity and vice-versa (for a review see [4]). Although the antimicrobial activity of NrTPs is out of the scope of the present work, it is definitely a worthwhile route for further studies. Also, the interaction with anionic membranes indicates that NrTPs may not be suitable for cargo delivery in prokaryotic cells, impairing their potential use as carriers for bacterial transformation.

3.5. Membrane leakage

Studies of membrane disturbance leading to leakage of an entrapped fluorescent probe from LUV were conducted for crotamine (up to 4 μM) with POPC vesicles, as well as for NrTP1 and NrTP5 (up to 20 μM) in the presence of POPC and POPG vesicles. These studies ruled out membrane disruption, as no significant leakage induced by crotamine or by the NrTPs was observed (percentage of leakage<2%; Fig. S11).

3.6. Circular dichroism

CD spectra were obtained for NrTP8 free in solution and in the presence of POPC or POPG LUV (Fig. 7). NrTP8 CD spectrum shows a unique negative band centered at 200 nm, characteristic of random-coil structures. Upon interaction with lipid vesicles, this large negative band, associated with the amide transition of disordered peptides, is replaced by another negative band, at 206 nm, typical of amide parallel transitions in the α-helix. A smaller positive band at 229 nm was also observed. A detailed spectral analysis of the CD spectra was made using the software K2d (http://www.embl.de/~andrade/k2d/; Table 5). The acquisition of secondary structure is evident within both POPC and POPG

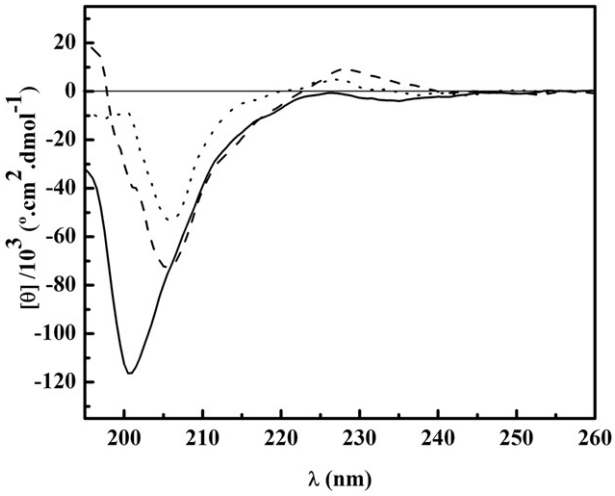

Fig. 7. Circular dichroism spectra of NrTP8 70 μM in solution (—), or in the presence of POPC (….) or POPG (——) 6 mM LUV.

membrane vesicles. The observed structural change should be associated with the establishment of Trp-phospholipid hydrogen bonds. Indeed, the short N-terminal α-helix in crotamine (residues 1–7) is stabilized by several hydrogen bonds, namely those between Tyr or Trp H_1 and Asp_{29} lateral chain (Fig. 1). We hypothesize that, upon interaction with the lipid, this bond can be restored, helping to stabilize the residues 1 to 9 region of the peptide. Possible hydrogen bond acceptors include lipid carbonyls and interfacial water molecules present near the phospholipid head-groups region [63].

3.7. Translocation assays

Translocation was tested for rhodamine B-labeled NrTP1 (NrTP1-RhB) and NrTP5 (NrTP5-RhB). The objective was to detect eventual translocation into the interior of lipid vesicles, as well as translocation across multiple lipid membranes. For both synthetic peptides, entry into the vesicles and accumulation in the membranes were clearly detected by confocal microscopy after approximately 20 min of incubation (Fig. 8). The co-localization of fluorescence spikes from NBD with those from RhB-labeled peptides in intravesicular membranes demonstrates an effective peptide translocation, as the labeled peptides crossed the external vesicle membrane in order to reach the inner membranes (smaller vesicles entrapped in the larger ones). From the approximately 60 vesicles analyzed (captured images), around 80% showed fluorescence in all the inner layers due to peptide internalization. NrTPs are soluble in water, and this property explains the higher values of background fluorescence detected in the aqueous media, when compared with NBD-PE. However, the peptide's preference for lipid membranes is evident from the fluorescence peaks observed on each bilayer (Fig. 8).

The lipid membrane system used in these experiments is deployed of any cellular component or electrochemical gradient, which compose the cellular machinery required for endocytic mechanisms. For this reason, direct translocation or membrane permeation has to be the overall mechanism (or one of the mechanisms) behind the translocation of

Table 5
Estimation of the percentages of NrTP8 secondary structure in the absence and presence of different lipids, calculated based on the UV circular dichroism data, using the K2d software (http://www.embl.de/~andrade/k2d/).

	Random coil	α-helix	β-sheet
NrTP8	99%	–	–
NrTP8-POPC	28%	33%	39%
NrTP8-POPG	28%	32%	40%

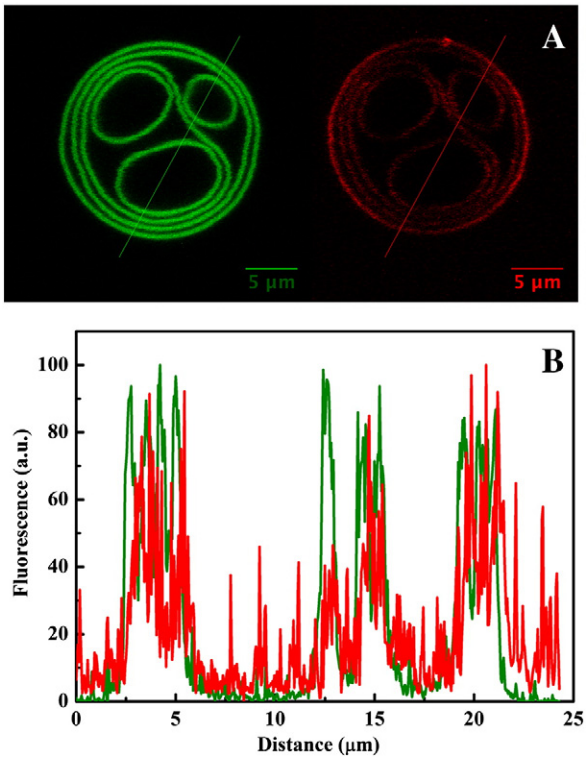

Fig. 8. Translocation of NrTP1-RhB into giant multivesicular liposomes and giant multilamellar vesicles (POPC + DPPE-NBD 1%), assessed by confocal microscopy. Panel B presents the normalized fluorescence intensities along a line drawn across the vesicle image (panel A), showing the co-localization of NBD (green; 488 nm laser) with NrTP1-RhB 15 µM (red; 561 nm laser). Each spike of the NBD fluorescence in B corresponds to a lipid bilayer.

NrTPs and their cargoes. Indeed, the detailed mechanism responsible for the passage of the peptide across a membrane is still not fully understood for most CPPs. However, endocytic-independent mechanisms of peptide entry are considered to play a significant role. Some models have been proposed to explain membrane permeation, including the inverted micelle [64], sinking-raft [65], carpet, the barrel stave pore and toroidal pore [66,67] models. These last two and the carpet model are often associated with the AMPs mechanism of action [68]. Based on our experimental evidences, we cannot be certain about the exact endocytosis-independent mechanism of NrTPs membrane translocation. Nevertheless, the inverted micelle model is a good candidate. Besides of being the model accepted to describe the internalization of several other CPPs, it is the model that predicts less membrane destabilization, which is consistent with the very low levels of toxicity observed for NrTPs. Results from leakage experiments also support this argument, since they exclude the formation of pores (either transient or permanent). It is worth noting that several CPPs have been shown to be able to enter cells by direct permeation, without the formation of pores in studies using GUV as membrane models [69]. Therefore, the inability of NrTPs to induce the formation of pores (absence of leakage), clearly distinguishes them from other peptides with antimicrobial activity.

Our confocal microscopy data clearly shows that, despite of the absence of electrochemical gradient or glycosaminoglycans (known mediators or facilitators of CPP uptake), translocation of NrTPs seemed to rely on a membrane partition-driven mechanism. Furthermore, it should be highlighted that, to the best of our knowledge, this is the first time this simple and direct methodology is used to assess peptide/protein translocation.

4. Conclusions

The present work unravels the molecular basis of the cell membrane translocation of NrTPs. Results show that the nucleolar targeting peptides have high affinity towards all the lipid membranes tested. As shown here, with both zwitterionic and negatively charged LUV, NrTPs revealed high K_p values. Quenching studies not only corroborate the partition data obtained, but also contribute for the assessment of peptide localization in the membrane. Together, these results reveal the ability of NrTPs to interact with zwitterionic vesicles, adsorbing on their lipid–water interface, retaining some degree of freedom to translocate across their membrane. Additionally, NrTPs insert on the hydrophobic interior of negatively-charged bilayers, which simulate bacterial membrane (Fig. 9).

Translocation studies showed that, besides interaction and penetration, these peptides are also able to translocate across lipid vesicle membranes. Remarkably, this demonstrates that the translocation and the concomitant CPP action are not dependent on the presence of specific receptors, such as glycosoaminoglycans (known to mediate the entry of many CPPs), or on the presence of electrochemical gradients.

In the present work, in addition to characterize and quantify the molecular determinants of NrTPs interaction with lipid membranes and their internalization into vesicles, the observed residual leakage of LUV-entrapped fluorophores indicates negligible toxic effects of NrTPs upon interaction and translocation across cell membranes.

It is known that the mechanisms by which CPPs translocate across lipid membranes and internalize into the cells differ from CPP to CPP, and sometimes between model systems, type of cells or nature of organisms and their tissues. Often the mechanism of peptide cell penetration depends on the CPP concentration, if the CPP is conjugated or un-conjugated, as well as on the peptide to cell ratio [68]. Therefore, an assertive conclusion about one exclusive and single mechanism of penetration is perhaps impossible. A more plausible explanation is that cell-penetrating peptides can use more than one route to gain access to the cell cytoplasm. The data presented here bring the awareness that the translocation of NrTPs can occur by the simplest of the models, i.e., membrane insertion and direct translocation. However, this does not exclude the possibility of other cell-specific mechanisms to be also involved on NrTPs translocation in more complex biological systems, as observed elsewhere for NrTP1, by our group [70].

The new methodology developed and applied by us to assess cell-penetrating peptide translocation based on the imaging of giant vesicles is simple, relatively fast and very informative.

All the studied NrTPs showed approximately the same trends regarding preference of interaction with different lipid membranes. The quantitative differences between peptides for their partition and quenching account for the variation in their amino acid sequence. Based on the results presented in this work, it is clear that all the tested NrTPs are potentially useful as nanoshuttles to carry compounds across lipid membranes. However, it is important to highlight that the presence of a spacer to connect the segments 1–9 and 38–42 of crotamine in the synthetic spliced peptides is apparently not an advantage. Importantly, an NrTP composed entirely of D-amino acid residues does not have its translocation impaired. This latter characteristic may improve the *in vivo* stability of the peptide.

We are sure that the understanding of the molecular interaction of NrTPs with lipid moieties, as presented and discussed in this work, associated with the mechanism of action of these peptides at the molecular level, constitute a critical step on the development of NrTPs as a valuable biomedical tool to ferry cargos into membrane-surrounded compartments. Our results show compelling evidences that NrTPs are promising CPPs, capable of interacting with lipid membranes of various compositions and translocate membranes by simple membrane intercalation and translocation without its disruption.

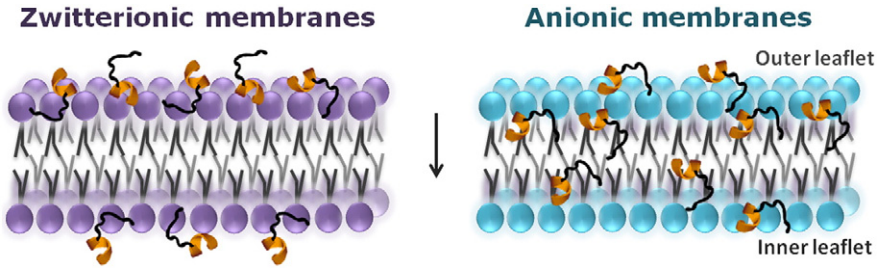

Fig. 9. Schematic illustration of NrTPs localization in lipid membranes. Results showed that NrTPs stay preferentially adsorbed on zwitterionic membranes, while in anionic membranes they are inserted in the membrane. Insertion of NrTPs in POPG containing vesicles is determined by the decrease in the K_{SV} observed for acrylamide quenching and by the higher K_{SV} values obtained with the lipophilic probes (5 and 16-NS), when compared with those obtained for zwitterionic lipid vesicles. Hence, in anionic membranes, NrTPs locate closer to the phospholipids acyl chains than in zwitterionic membranes. On the other hand, the unchanged K_{SV} for acrylamide quenching in the presence of POPC membranes shows that most of the peptide must stay adsorbed, fully accessible to the quencher. The fact that NrTPs quenching by both 5 and 16-NS probes was similar (but lower than for POPG) can be explained by the broader in-depth membrane localization of 16-NS in the membrane, which generates a misleading higher value of K_{SV} for 16-NS.

Supplementary data to this article can be found online at http://dx.doi.org/10.1016/j.bbamem.2012.06.014.

Acknowledgements

The authors thank Miguel Castanho (IMM) for valuable discussions, to Ivo C. Martins (IMM) for support on the circular dichroism experiments, and to Bruno Castro (IST, Technical University of Lisbon) for the help on GUV preparation. This work was funded by the Portuguese Ministry of Education and Science (Fundação para a Ciência e a Tecnologia, FCT-MEC; including M.R. and A.S. fellowships SFRH/BD/37432/2007 and SFRH/BPD/26821/2006, respectively), the Spanish Ministry of Economy and Competitiveness (MINECO, grant SAF2011-24899), Generalitat de Catalunya (2009 SGR 492), FP7-PEOPLE IRSES (International Research Staff Exchange Scheme) project MEMPEPACROSS (European Union), and the European Biophysical Societies' Association (EBSA).

References

[1] A.D. Frankel, C.O. Pabo, Cellular uptake of the tat protein from human immunodeficiency virus, Cell 55 (1988) 1189–1193.
[2] E. Vives, Present and future of cell-penetrating peptide mediated delivery systems: "is the Trojan horse too wild to go only to Troy?", J. Control. Release 109 (2005) 77–85.
[3] P. Jarver, I. Mager, U. Langel, In vivo biodistribution and efficacy of peptide mediated delivery, Trends Pharmacol. Sci. 31 (2010) 528–535.
[4] S.T. Henriques, M.N. Melo, M.A.R.B. Castanho, Cell-penetrating peptides and antimicrobial peptides: how different are they? Biochem. J. 399 (2006) 1–7.
[5] K.M. Stewart, K.L. Horton, S.O. Kelley, Cell-penetrating peptides as delivery vehicles for biology and medicine, Org. Biomol. Chem. 6 (2008) 2242–2255.
[6] R.M. Martin, G. Tunnemann, H. Leonhardt, M.C. Cardoso, Nucleolar marker for living cells, Histochem. Cell Biol. 127 (2007) 243–251.
[7] S.T. Henriques, M.A.R.B. Castanho, Environmental factors that enhance the action of the cell penetrating peptide pep-1. A spectroscopic study using lipidic vesicles, Biochim. Biophys. Acta 1669 (2005) 75–86.
[8] R.M. Johnson, S.D. Harrison, D. Maclean, Therapeutic applications of cell-penetrating peptides, Methods Mol. Biol. 683 (2010) 535–551.
[9] B.R. Meade, S.F. Dowdy, Exogenous siRNA delivery using peptide transduction domains/cell penetrating peptides, Adv. Drug Deliv. Rev. 59 (2007) 134–140.
[10] J.R. Luque-Ortega, B.G. De la Torre, V. Hornillos, J.M. Bart, C. Rueda, M. Navarro, F. Amat-Guerri, A.U. Acuña, D. David Andreu, L. Rivas, Defeating Leishmania resistance to Miltefosine (hexadecylphosphocholine) by peptide-mediated drug smuggling: a proof of mechanism for trypanosomatid chemotherapy, J. Control. Release (May 18 2012) [Electronic publication ahead of print].
[11] A. Joliot, C. Pernelle, H. Deagostini-Bazin, A. Prochiantz, Antennapedia homeobox peptide regulates neural morphogenesis, Proc. Natl. Acad. Sci. U. S. A. 88 (1991) 1864–1868.
[12] G. Elliott, P. O'Hare, Intercellular trafficking and protein delivery by a herpesvirus structural protein, Cell 88 (1997) 223–233.
[13] A. Kerkis, I. Kerkis, G. Radis-Baptista, E.B. Oliveira, A.M. Vianna-Morgante, L.V. Pereira, T. Yamane, Crotamine is a novel cell-penetrating protein from the venom of rattlesnake *Crotalus durissus terrificus*, FASEB J. 18 (2004) 1407–1409.
[14] V. Fadel, P. Bettendorff, T. Herrmann, W.F. de Azevedo Jr., E.B. Oliveira, T. Yamane, K. Wuthrich, Automated NMR structure determination and disulfide bond identification of the myotoxin crotamine from *Crotalus durissus terrificus*, Toxicon 46 (2005) 759–767.
[15] D.M. Hoover, O. Chertov, J. Lubkowski, The structure of human beta-defensin-1: new insights into structural properties of beta-defensins, J. Biol. Chem. 276 (2001) 39021–39026.
[16] A.M. Torres, G.M. de Plater, M. Doverskog, L.C. Birinyi-Strachan, G.M. Nicholson, C.H. Gallagher, P.W. Kuchel, Defensin-like peptide-2 from platypus venom: member of a class of peptides with a distinct structural fold, Biochem. J. 348 (2000) 649–656.
[17] D. Housset, C. Habersetzer-Rochat, J.P. Astier, J.C. Fontecilla-Camps, Crystal structure of toxin II from the scorpion *Androctonus australis* Hector refined at 1.3 A resolution, J. Mol. Biol. 238 (1994) 88–103.
[18] A.M. Siqueira, N.F. Martins, M.E. De Lima, C.R. Diniz, A. Cartier, D. Brown, B. Maigret, A proposed 3D structure for crotamine based on homology building, molecular simulations and circular dichroism, J. Mol. Graph. Model. 20 (2002) 389–398.
[19] G. Rádis-Baptista, B.G. de la Torre, D. Andreu, A novel cell-penetrating peptide sequence derived by structural minimization of a snake toxin exhibits preferential nucleolar localization, J. Med. Chem. 51 (2008) 7041–7044.
[20] M. Rodrigues, B.G. de la Torre, G. Rádis-Baptista, N.C. Santos, D. Andreu, Efficient cellular delivery of β-galactosidase mediated by NrTPs, a new family of cell-penetrating peptides, Bioconjugate Chem. 22 (2011) 2339–2344.
[21] M. Vila-Perello, A. Sanchez-Vallet, F. Garcia-Olmedo, A. Molina, D. Andreu, Synthetic and structural studies on *Pyrularia pubera* thionin: a single-residue mutation enhances activity against Gram-negative bacteria, FEBS Lett. 536 (2003) 215–219.
[22] S. Fery-Forgues, L. Dominique, Are fluorescence quantum yields so tricky to measure? A demonstration using familiar stationery products, J. Chem. Educ. 76 (1999) 1260–1264.
[23] L.D. Mayer, M.J. Hope, P.R. Cullis, Vesicles of variable sizes produced by a rapid extrusion procedure, Biochim. Biophys. Acta 858 (1986) 161–168.
[24] R.F. de Almeida, J. Borst, A. Fedorov, M. Prieto, A.J. Visser, Complexity of lipid domains and rafts in giant unilamellar vesicles revealed by combining imaging and microscopic and macroscopic time-resolved fluorescence, Biophys. J. 93 (2007) 539–553.
[25] B.M. Castro, L.C. Silva, A. Fedorov, R.F. de Almeida, M. Prieto, Cholesterol-rich fluid membranes solubilize ceramide domains: implications for the structure and dynamics of mammalian intracellular and plasma membranes, J. Biol. Chem. 284 (2009) 22978–22987.
[26] N. Rodriguez, F. Pincet, S. Cribier, Giant vesicles formed by gentle hydration and electroformation: a comparison by fluorescence microscopy, Colloids Surf. B Biointerfaces 42 (2005) 125–130.
[27] A.S. Ladokhin, S. Jayasinghe, S.H. White, How to measure and analyze tryptophan fluorescence in membranes properly, and why bother? Anal. Biochem. 285 (2000) 235–245.
[28] N.C. Santos, M. Prieto, M.A.R.B. Castanho, Quantifying molecular partition into model systems of biomembranes: an emphasis on optical spectroscopic methods, Biochim. Biophys. Acta 1612 (2003) 123–135.
[29] P.M. Matos, H.G. Franquelim, M.A.R.B. Castanho, N.C. Santos, Quantitative assessment of peptide–lipid interactions. Ubiquitous fluorescence methodologies, Biochim. Biophys. Acta 1798 (2010) 1999–2012.
[30] M.M. Ribeiro, M.N. Melo, I.D. Serrano, N.C. Santos, M.A. Castanho, Drug–lipid interaction evaluation: why a 19th century solution? Trends Pharmacol. Sci. 31 (2010) 449–454.
[31] A. Coutinho, M. Prieto, Ribonuclease T1 and alcohol dehydrogenase fluorescence quenching by acrylamide, J. Chem. Educ. 70 (1993) 1–4.
[32] J.R. Lakowicz, Principles of Fluorescence Spectroscopy, Springer, Singapore, 2006.
[33] S.S. Lehrer, Solute perturbation of protein fluorescence. The quenching of the tryptophyl fluorescence of model compounds and of lysozyme by iodide ion, Biochemistry 10 (1971) 3254–3263.
[34] D.E. Chalpin, A.M. Kleinfeld, Interaction of fluorescence quenchers with the n-(9-anthroyloxy) fatty acid membrane probes, Biochim. Biophys. Acta 731 (1983) 465–474.
[35] I.M. Frank, S.I. Vavilov, Über die wirkungssphäre der aus-löschuns-vargänge in den flureszierenden flussig-keiten, Z. Phys. 69 (1931) 100–110.
[36] D.W. Marquardt, An algorithm for least-squares estimation of nonlinear parameters, J. Soc. Ind. Appl. Math. 11 (1963) 431–441.

[37] N.C. Santos, M. Prieto, M.A.R.B. Castanho, Interaction of the major epitope region of HIV protein gp41 with membrane model systems. A fluorescence spectroscopy study, Biochemistry 37 (1998) 8674–8682.
[38] J.R. Wardlaw, W.H. Sawyer, K.P. Ghiggino, Vertical fluctuations of phospholipid acyl chains in bilayers, FEBS Lett. 223 (1987) 20–24.
[39] S.W. Provencher, A constrained regularization method for inverting data represented by linear algebraic or integral equations, Comput. Phys. Commun. 27 (1982) 213–227.
[40] S.W. Provencher, CONTIN: a general-purpose constrained regularization program for inverting data represented by linear algebraic and integral-equations, Comput. Phys. Commun. 27 (1982) 229–242.
[41] M.M. Domingues, M.A.R.B. Castanho, N.C. Santos, $rBPI_{21}$ promotes lipopolysaccharide aggregation and exerts its antimicrobial effects by (hemi)fusion of PG-containing membranes, PLoS One 4 (2009) e8385.
[42] J.N. Weinstein, R.D. Klausner, T. Innerarity, E. Ralston, R. Blumenthal, Phase transition release, a new approach to the interaction of proteins with lipid vesicles. Application to lipoproteins, Biochim. Biophys. Acta 647 (1981) 270–284.
[43] R.W. Woody, Circular dichroism, Methods Enzymol. 246 (1995) 34–71.
[44] M.A. Andrade, P. Chacon, J.J. Merelo, F. Moran, Evaluation of secondary structure of proteins from UV circular dichroism spectra using an unsupervised learning neural network, Protein Eng. 6 (1993) 383–390.
[45] J.B.A. Ross, W.R. Laws, K.W. Rousslang, H.R. Wyssbrod, Tyrosine fluorescence and phosphorescence from proteins and polypeptides, In: in: J.R. Lakowicz (Ed.), Topics in Fluorescence Spectroscopy - Biochemical Applications, vol. 3, Plenum Press, New York, 1992, pp. 1–63.
[46] R.F. de Almeida, A. Fedorov, M. Prieto, Sphingomyelin/phosphatidylcholine/cholesterol phase diagram: boundaries and composition of lipid rafts, Biophys. J. 85 (2003) 2406–2416.
[47] J.L. Thewalt, M. Bloom, Phosphatidylcholine: cholesterol phase diagrams, Biophys. J. 63 (1992) 1176–1181.
[48] C. Reyes Mateo, A. Ulises Acuna, J.C. Brochon, Liquid-crystalline phases of cholesterol/lipid bilayers as revealed by the fluorescence of trans-parinaric acid, Biophys. J. 68 (1995) 978–987.
[49] D. Marsh, Liquid-ordered phases induced by cholesterol: a compendium of binary phase diagrams, Biochim. Biophys. Acta 1798 (2010) 688–699.
[50] D. Marsh, Handbook of Lipid Bilayers, CRC Press, Boca Raton, FL, 1990.
[51] R.B. Gennis, Biomembranes: Molecular Structure and Function, Springer-Verlag, New York, 1989.
[52] K. Matsuzaki, K. Sugishita, M. Harada, N. Fujii, K. Miyajima, Interactions of an antimicrobial peptide, magainin 2, with outer and inner membranes of Gram-negative bacteria, Biochim. Biophys. Acta 1327 (1997) 119–130.
[53] G. Fujii, D. Eisenberg, M.E. Selsted, Defensins promote fusion and lysis of negatively charged membranes, Prot. Sci. 2 (1993) 1301–1312.
[54] S. Goncalves, A. Teixeira, J. Abade, L.N. de Medeiros, E. Kurtenbach, N.C. Santos, Evaluation of the membrane lipid selectivity of the pea defensin Psd1, Biochim. Biophys. Acta 1818 (2011) 1420–1426.
[55] Y. Chen, M.D. Barkley, Toward understanding tryptophan fluorescence in proteins, Biochemistry 37 (1998) 9976–9982.
[56] F. Moro, F.M. Goñi, M.A. Urbaneja, Fluorescence quenching at interfaces and the permeation of acrylamide and iodide across phospholipid bilayers, FEBS Lett. 330 (1993) 129–132.
[57] H.G. Franquelim, A.S. Veiga, G. Weissmüller, N.C. Santos, M.A. Castanho, Unravelling the molecular basis of the selectivity of the HIV-1 fusion inhibitor sifuvirtide towards phosphatidylcholine-rich rigid membranes, Biochim. Biophys. Acta 1798 (2010) 1234–1243.
[58] A. Chattopadhyay, E. London, Parallax method for direct measurement of membrane penetration depth utilizing fluorescence quenching by spin-labeled phospholipids, Biochemistry 26 (1987) 39–45.
[59] M. Castanho, M. Prieto, A.U. Acuna, The transverse location of the fluorescent probe trans-parinaric acid in lipid bilayers, Biochim. Biophys. Acta 1279 (1996) 164–168.
[60] M.X. Fernandes, J. Garcia de la Torre, M.A. Castanho, Joint determination by Brownian dynamics and fluorescence quenching of the in-depth location profile of biomolecules in membranes, Anal. Biochem. 307 (2002) 1–12.
[61] M.R. Eftink, C.A. Ghiron, Fluorescence quenching of indole and model micelle systems, J. Phys. Chem. 80 (1976) 488–493.
[62] N.C. Santos, A.C. Silva, M.A.R.B. Castanho, J. Martins-Silva, C. Saldanha, Evaluation of lipopolysaccharide aggregation by light scattering spectroscopy, Chembiochem 4 (2003) 96–100.
[63] S. Mukherjee, A. Chattopadhyay, Motionally restricted tryptophan environments at the peptide–lipid interface of gramicidin channels, Biochemistry 33 (1994) 5089–5097.
[64] A. Prochiantz, Messenger proteins: homeoproteins, TAT and others, Curr. Opin. Cell Biol. 12 (2000) 400–406.
[65] A. Pokorny, P.F. Almeida, Kinetics of dye efflux and lipid flip-flop induced by delta-lysin in phosphatidylcholine vesicles and the mechanism of graded release by amphipathic, alpha-helical peptides, Biochemistry 43 (2004) 8846–8857.
[66] B. Geueke, K. Namoto, I. Agarkova, J.C. Perriard, H.P. Kohler, D. Seebach, Bacterial cell penetration by beta3-oligohomoarginines: indications for passive transfer through the lipid bilayer, Chembiochem 6 (2005) 982–985.
[67] S. Trabulo, A.L. Cardoso, M. Mano, M.C.P. Lima, Cell-penetrating peptides-mechanisms of cellular uptake and generation of delivery systems, Pharmaceuticals 3 (2010) 961–993.
[68] R. Fischer, M. Fotin-Mleczek, H. Hufnagel, R. Brock, Break on through to the other side-biophysics and cell biology shed light on cell-penetrating peptides, Chembiochem 6 (2005) 2126–2142.
[69] P.E. Thoren, D. Persson, E.K. Esbjorner, M. Goksor, P. Lincoln, B. Norden, Membrane binding and translocation of cell-penetrating peptides, Biochemistry 43 (2004) 3471–3489.
[70] G. Radis-Baptista, B.G. de la Torre, D. Andreu, Insights into the uptake mechanism of NrTP, a cell-penetrating peptide preferentially targeting the nucleolus of tumour cells, Chem. Biol. Drug Des. 79 (2012) 907–915.